Dislocation density dependent electroabsorption in epitaxial lateral overgrown InGaN/GaN quantum structures

Emre Sari,[1,2] Lee Woon Jang,[3] Jong Hyeob Baek,[4] In Hwan Lee,[3] Xiao Wei Sun,[2] and Hilmi Volkan Demir[1,2,*]

[1]*Department of Electrical and Electronics Engineering, Department of Physics, UNAM-National Nanotechnology Research Center, Bilkent University, 06800 Bilkent, Ankara, Turkey*
[2]*School of Electrical and Electronic Engineering, Microelectronics Division; School of Physical and Mathematical Sciences, Physics and Applied Physics Division, Nanyang Technological University, Singapore 639798, Singapore*
[3]*School of Advanced Materials Engineering, Research Center of Industrial Technology, Chonbuk National University, Chonju 561-756, South Korea*
[4]*Korea Photonics Technology Institute, Gwangju, 500-460, South Korea*
**volkan@stanfordalumni.org*

Abstract: We study electroabsorption (EA) behavior of InGaN/GaN quantum structures grown using epitaxial lateral overgrowth (ELOG) in correlation with their dislocation density levels and in comparison to steady state and time-resolved photoluminescence measurements. The results reveal that ELOG structures with decreasing mask stripe widths exhibit stronger EA performance, with a maximum EA enhancement factor of 4.8 compared to the reference without ELOG. The analyses show that the EA performance follows similar trends with decreasing dislocation density as the essential parameters of the photoluminescence spectra (peak position, width and intensity) together with the photoluminescence lifetimes. While keeping the growth window widths constant, compared to photoluminescence behavior, however, EA surprisingly exhibits the largest performance variation, making EA the most sensitive to the mask stripe widths.

OCIS codes: (160.4760) Optical properties; (160.6000) Semiconductor materials; (230.0250) Optoelectronics.

References and links

1. H. Zhao, G. Liu, J. Zhang, J. D. Poplawsky, V. Dierolf, and N. Tansu, "Approaches for high internal quantum efficiency green InGaN light-emitting diodes with large overlap quantum wells," Opt. Express **19**(S4 Suppl 4), A991–A1007 (2011).
2. S. P. Denbaars, "Gallium-nitride-based materials for blue to ultraviolet optoelectronics devices," Proc. IEEE **85**(11), 1740–1749 (1997).
3. C.-Y. Cho, J.-B. Lee, S.-J. Lee, S.-H. Han, T.-Y. Park, J. W. Kim, Y. C. Kim, and S.-J. Park, "Improvement of light output power of InGaN/GaN light-emitting diode by lateral epitaxial overgrowth using pyramidal-shaped SiO_2," Opt. Express **18**(2), 1462–1468 (2010).
4. C. Bayram, J. L. Pau, R. McClintock, and M. Razeghi, "Comprehensive study of blue and green multi-quantum-well light emitting diodes grown on conventional and lateral epitaxial overgrowth GaN," Appl. Phys. B **95**(2), 307–314 (2009).
5. S. Nakamura, "The roles of structural imperfections in InGaN-based blue light-emitting diodes and laser diodes," Science **281**(5379), 956–961 (1998).
6. P. Gibart, "Metal organic vapour phase epitaxy of GaN and lateral overgrowth," Rep. Prog. Phys. **67**(5), 667–715 (2004).
7. S. Nakamura, M. Senoh, S. Nagahama, N. Iwasa, T. Yamada, T. Matsushita, H. Kiyoku, Y. Sugimoto, T. Kozaki, H. Umemoto, M. Sano, and K. Chocho, "InGaN/GaN/AlGaN-based laser diodes with modulation-doped strained-layer superlattices grown on an epitaxially laterally overgrown GaN substrate," Appl. Phys. Lett. **72**(2), 211–213 (1998).
8. A. Usui, H. Sunakawa, A. Sakai, and A. A. Yamaguchi, "Thick GaN epitaxial growth with low dislocation density by hydride vapor phase epitaxy," Jpn. J. Appl. Phys. **36**(Part 2, No. 7B), L899–L902 (1997).
9. C. F. Johnston, M. A. Moram, M. J. Kappers, and C. J. Humphreys, "Defect reduction in (11-22) semipolar GaN grown on m-plane sapphire using ScN interlayers," Appl. Phys. Lett. **94**(16), 161109 (2009).

#176411 - $15.00 USD Received 18 Sep 2012; revised 15 Nov 2012; accepted 13 Dec 2012; published 10 Jan 2013

10. B. M. Imer, F. Wu, S. P. DenBaars, and J. S. Speck, "Improved quality (11-20) a-plane GaN with sidewall lateral epitaxial overgrowth," Appl. Phys. Lett. **88**(6), 061908 (2006).
11. C. Y. Huang, H. M. Ku, C. Z. Liao, and S. Chao, "MQWs InGaN/GaN LED with embedded micro-mirror array in the epitaxial-lateral-overgrowth gallium nitride for light extraction enhancement," Opt. Express **18**(10), 10674–10684 (2010).
12. D. A. B. Miller, D. S. Chemla, T. C. Damen, A. C. Gossard, W. Wiegmann, T. H. Wood, and C. A. Burrus, "Electric field dependence of optical absorption near the bandgap of quantum well Structures," Phys. Rev. B **32**(2), 1043–1060 (1985).
13. H. V. Demir, V. A. Sabnis, O. Fidaner, J. S. Harris, Jr., D. A. B. Miller, and J.-F. Zheng, "Dual-diode quantum-well modulator for C-band wavelength conversion and broadcasting," Opt. Express **12**(2), 310–316 (2004).
14. H. V. Demir, V. A. Sabnis, O. Fidaner, J.-F. Zheng, J. S. Harris, Jr., and D. A. B. Miller, "Multifunctional integrated photonic switches," IEEE J. Sel. Top. Quantum Electron. **11**(1), 86–96 (2005).
15. E. Sari, S. Nizamoglu, T. Ozel, and H. V. Demir, "Blue quantum electroabsorption modulators based on reversed quantum confined Stark effect with blueshift," Appl. Phys. Lett. **90**(1), 011101 (2007).
16. I. Friel, C. Thomidis, and T. D. Moustakas, "Ultraviolet electroabsorption modulator based on AlGaN/GaN multiple quantum wells," J. Appl. Phys. **97**(12), 123515 (2005).
17. A. Bhatnagar, S. Latif, C. Debaes, and D. A. B. Miller, "Pump-probe measurements of CMOS detector rise time in the blue," J. Lightwave Technol. **22**(9), 2213–2217 (2004).
18. Z. Xu, G. Chen, F. Abou-Galala, and M. Leonardi, "Experimental performance evaluation of non-line-of-sight ultraviolet communication systems," Proc. SPIE **6709**, 67090Y (2007).
19. I.-L. Lu, Y.-R. Wu, and J. Singh, "A study of the role of dislocation density, indium composition on the radiative efficiency in InGaN/GaN polar and nonpolar light-emitting diodes using drift-diffusion coupled with a Monte Carlo method," J. Appl. Phys. **108**(12), 124508 (2010).
20. M. F. Schubert, S. Chhajed, J. K. Kim, E. F. Schubert, D. D. Koleske, M. H. Crawford, S. R. Lee, A. J. Fischer, G. Thaler, and M. A. Banas, "Effect of dislocation density on efficiency droop in GaInN/GaN light-emitting diodes," Appl. Phys. Lett. **91**(23), 231114 (2007).
21. E. Sari, S. Nizamoglu, I.-H. Lee, J.-H. Baek, and H. V. Demir, "Electric field dependent radiative decay kinetics of polar InGaN/GaN quantum heterostructures at low fields," Appl. Phys. Lett. **94**(21), 211107 (2009).
22. S.-M. Kim, H. S. Oh, J. H. Baek, K.-H. Lee, G. Y. Jung, J.-H. Song, H.-J. Kim, B.-J. Ahn, D. Yanqun, and J.-H. Song, "Effects of patterned sapphire substrates on piezoelectric field in blue-emitting InGaN multiple quantum wells," IEEE Electron Device Lett. **31**(8), 842–844 (2010).
23. S. J. Tu, J. K. Sheu, M. L. Lee, C. C. Yang, K. H. Chang, Y. H. Yeh, F. W. Huang, and W. C. Lai, "Enhanced output power of GaN-based LEDs with embedded AlGaN pyramidal shells," Opt. Express **19**(13), 12719–12726 (2011).
24. L. Y. Chen, H. H. Huang, C. H. Chang, Y. Y. Huang, Y. R. Wu, and J. J. Huang, "Investigation of the strain induced optical transition energy shift of the GaN nanorod light emitting diode arrays," Opt. Express **19**(S4 Suppl 4), A900–A907 (2011).

1. Introduction

GaN-based optoelectronic devices, e.g., light-emitting diodes (LEDs) and laser diodes (LDs), serve as the enabling technology platforms finding critical use in important applications including indoor and outdoor lighting, liquid crystal display (LCD) backlighting, and data storage. Today efforts essential to the improvement of device performance in these applications still continue through exploiting materials science and device engineering [1]. One of the main efforts in the field is targeted towards obtaining large-area GaN substrates for the homoepitaxy of these devices at a reduced cost, aiming to achieve a high crystal quality for a better device performance, a longer lifetime, and ultimately a deeper market penetration. However, since obtaining these native substrates commonly requires expensive and difficult processes, they have not thus far been used at a scale as widely as anticipated. Although there have been studies on utilizing different substrates for GaN epitaxial growth, sapphire (Al_2O_3) is still the most widely used substrate material in both scientific research and mass production of related devices such as LEDs [2].

However, common to all non-native substrates of GaN, sapphire exhibits a large crystal lattice mismatch (about 14%), forming dislocations in the epitaxy as a result of the relaxation of the strain induced during the epitaxial growth. For the state-of-the-art bulk templates (those grown with the traditional nucleation layer approach, i.e., epi-growth directly on sapphire), e.g., in commercial LEDs, defect densities still remain in the range of 10^8 cm^{-2}. The typical levels are, however, estimated to be in the 10^9 cm^{-2} range [3–5]. Further reduction of the defect densities requires special techniques for the relaxation of strain and/or termination of defects formed during the growth [6].

#176411 - $15.00 USD Received 18 Sep 2012; revised 15 Nov 2012; accepted 13 Dec 2012; published 10 Jan 2013

Epitaxial lateral overgrowth (ELOG), which is based on selective area growth, is one of the most powerful techniques for the reduction of threading dislocation densities, thus enabling substantial improvement in the crystal quality of GaN material system [5]. Under proper conditions, ELOG results in smooth surfaces with low defect densities by blocking propagation of the defects underneath the hard mask, usually defined by Si_3N_4 or SiO_2 on a GaN template. This involves lateral growth over the mask, hence preventing the defects from propagating to the surface and leading to a surface with significantly fewer defects for the growth of subsequent layers [6]. As investigated by several groups studying photoluminescence properties to date, ELOG has proven to be a successful method to improve GaN material quality as well as the performance of resulting optoelectronic devices including LEDs [4] and LDs [7] when grown on polar [8], semipolar [9] and nonpolar [10] directions of their crystals. ELOG-LEDs with embedded micro mirror arrays have also been demonstrated to further improve the light extraction efficiency [11].

In terms of understanding the underpinning physical mechanisms, electroabsorption offers a unique means to explore and understand physics of semiconductor structures. This is especially the case for quantum-confined structures, which exhibit electroabsorption exceptionally stronger than their bulk counterparts through quantum-confined Stark effect (QCSE) [12]. Electroabsorption modulators that utilize QCSE have found applications in telecommunications in the last few decades, e.g., in data coding [13] and optical switching [14]. Most of these studies involved InP/GaAs material system, and the operation wavelength of these devices has therefore been typically in the mid-infrared part of the electromagnetic spectrum. On the other hand, electroabsorption modulators based on III-Nitride quantum structures, which operate in the blue [15] and ultraviolet [16] region of the electromagnetic spectrum, were also demonstrated. These find applications in optical clock injection directly into silicon chips [17] and none-of-sight communications [18]. However, electroabsorption in InGaN/GaN quantum structures grown on ELOG-GaN has not been investigated to date.

Here in this paper, we report electroabsorption performance of epitaxial lateral overgrown InGaN/GaN quantum structures, in comparison to their steady-state and time-resolved photoluminescence properties, and correlate our results with the dislocation density levels. In this study, we employ a set of four epi-structures, three of which are designed to contain systematically varying ELOG mask stripe widths while the last one is used as a reference sample without ELOG.

2. Epitaxial growth and device fabrication

Our epitaxial structures were grown using metal-organic chemical vapor deposition (MOCVD). After the growth of 5 μm thick u-GaN templates on single side polished sapphire substrates, we deposited and defined SiO_2 stripe patterns all in (0-100) direction. The width of the SiO_2 stripe masks is varied to be 4, 7 and 10 μm, whereas that of the unmasked window regions is kept constant at 4 μm for the three samples containing ELOG stripe patterns. No patterning was used for the fourth sample, which serves as the reference. We followed a standard single step ELOG procedure [5]. The lateral growth time was sufficiently long for each of our samples to completely coalesce in the middle-top part of the mask regions. After the coalescence, we changed the growth mode to vertical growth to obtain 2 μm thick Si doped n-type GaN layer ($N_{Si} \approx 4 \times 10^{18}$ cm^{-3}) and InGaN/GaN multiple quantum well (MQW) structure with 5 pairs of well and barriers having thicknesses of 2.5 and 7.5 nm, respectively. After the growth of the MQW, we continued with Mg-doped 150 nm thick p-GaN layer ($N_{Mg} \approx 6 \times 10^{17}$ cm^{-3}) and completed the epi-samples.

We fabricated devices using these ELOG and reference epi-samples utilizing standard photolithography, mesa etching and metallization procedures. The fabrication and subsequent characterization of the devices were performed under the same conditions, all with identical settings and parameters. The mesa size of the resulting devices is 300 μm × 300 μm. These devices allowed us to apply external bias and extract photocurrent for electroabsorption study (in the case of reverse biasing).

#176411 - $15.00 USD Received 18 Sep 2012; revised 15 Nov 2012; accepted 13 Dec 2012; published 10 Jan 2013

3. Results and discussions

Following the MOCVD ELOG growth of our samples, we measured the dislocation densities through forming etch pits using wet etching and investigating scanning electron microscopy (SEM) images presented in Figs. 1(a)–1(d). Our analyses showed that the etch pit density for the reference sample was the highest and that of the ELOG sample with 4 μm wide stripes was the lowest, with the respective values of 3.25×10^8 and 0.88×10^8 cm^{-2}. The etch pit densities of the other ELOG structures with 7 and 10 μm wide stripes were 1.84×10^8 and 1.58×10^8 cm^{-2}, respectively.

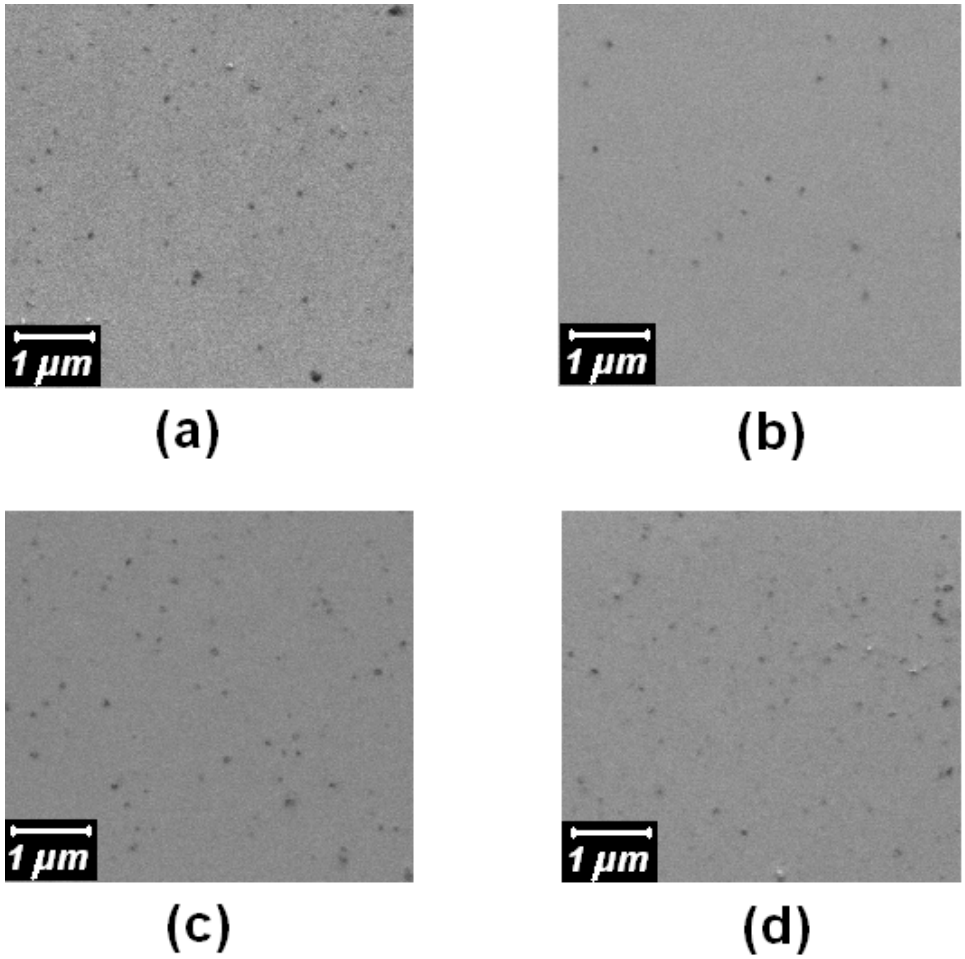

Fig. 1. Representative parts of the analyzed scanning electron microscopy images of the top surface of our epi-structures after etch pit formation: (a) reference sample, and ELOG samples with (b) 4 μm, (c) 7 μm, and (d) 10 μm wide stripes.

In addition, we performed photoluminescence (PL) measurements using our setup containing a He-Cd laser at 325 nm, an optical microscope with a high magnifying power (100 ×) objective lens and a motorized stage, a monochromator, and a broadband photodetector. We carefully set the position and spot size (~2 μm) of the incoming laser beam properly such that all photons that contribute to the PL signal come from the low dislocation density region of the epitaxy. PL spectra corresponding to the Reference sample and the ELOG samples are given in Figs. 2(a)–2(d).

#176411 - $15.00 USD Received 18 Sep 2012; revised 15 Nov 2012; accepted 13 Dec 2012; published 10 Jan 2013

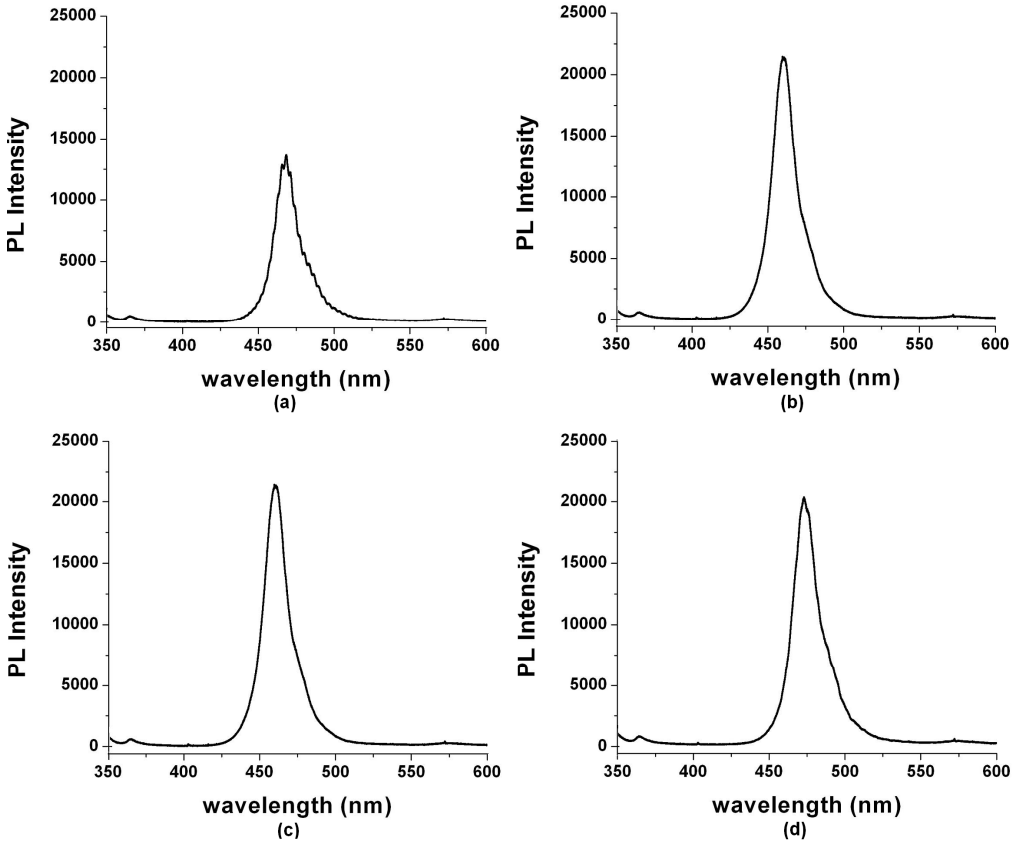

Fig. 2. PL spectra of (a) reference sample, and ELOG samples with (b) 4 μm, (c) 7 μm and (d) 10 μm wide stripes.

As a result of our PL measurements, we found that the PL peak emission wavelengths (λ_{PL}) were in the range of 466 ± 7 nm. This confirms that the levels of InN incorporated in the well regions of the MQW layers were similar to each other. Specifically, the structure with 4 μm wide stripes emit at the shortest wavelength, λ_{PL}, with the highest peak intensity, I_{PL}. Moreover, the FWHM of the PL spectra, $\Delta\lambda_{PL}$, was the lowest for the reference sample (18.47 nm), and very close to the sample with 4 μm stripes (18.53 nm). These results indicate that the Reference sample exhibits the weakest PL. (All important parameters of these PL spectra, which will later be discussed again to be compared against EA characterization results.)

Moreover, we performed time-resolved photoluminescence (TRPL) measurements for studying the carrier generation rate in the quantum structures. We used PicoQuant time-resolved photoluminescence setup comprising an InGaN-based laser diode operated at 375 nm in pulsed mode, with the monochromator center wavelength set at 466 nm in the photon collection side, for all of the samples. We fit the decay curves with three exponentials to obtain the minimum deviation from the actual data and considered the carrier recombination rates, R_i, as the reciprocal of the intensity averaged lifetimes, τ_i^{-1}. We present the experimental TRPL decay curves of the four structures and the instrument response function (IRF), along with their numerical fits in Fig. 3. In our fitting procedure, we deconvolve IRF from the actual decay data to extract photoluminescence lifetimes.

#176411 - $15.00 USD Received 18 Sep 2012; revised 15 Nov 2012; accepted 13 Dec 2012; published 10 Jan 2013

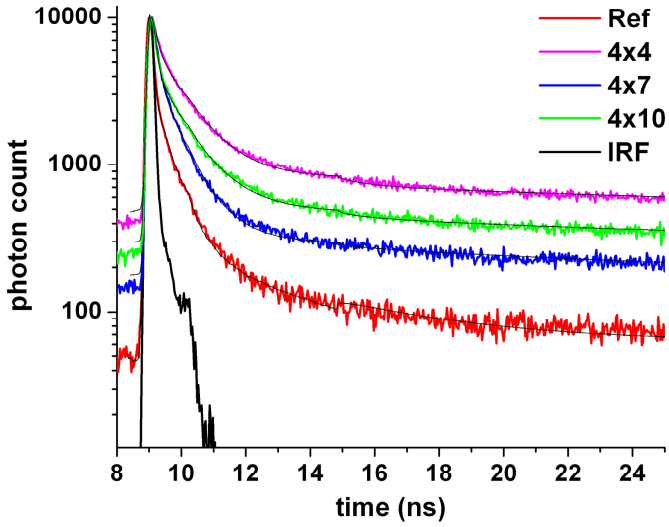

Fig. 3. Time-resolved photoluminescence decay profiles of our epitaxial lateral overgrowth structures and the reference sample along with their corresponding fits. The fastest decay profile corresponds to the reference sample due to its higher dislocation density, and thus higher nonradiative recombination rate. The instrument response function (IRF) is denoted by the black decay curve.

The extracted recombination rates correlate well with the dislocation density levels in our epi-structures, considering the fact that the dislocations form nonradiative recombination centers, increasing the nonradiative recombination rate and, thus, the overall recombination rate. As a result, the recombination rates, measured using TRPL, should exhibit a similar trend with the dislocation densities, at least when the dislocation densities are significantly different, which is the case for the Reference sample and the ELOG sample with 4 μm wide stripes, as shown in Figs. 4(a) and 4(b). These results are also consistent with the previous theoretical [19] and experimental [20] studies.

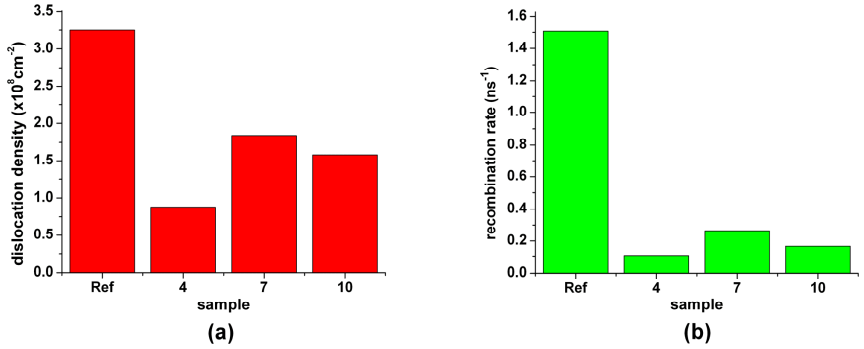

Fig. 4. Comparison of (a) dislocation densities measured by SEM analysis and (b) recombination rates of our structures measured by TRPL analysis.

We further performed photocurrent measurements at different levels of reverse bias applied across our devices and recorded the field dependent change in the photocurrent, which corresponds to the electroabsorption of the samples under test. Our photocurrent setup consists of a broadband Xenon lamp, a monochromator, an optical chopper, a lock-in amplifier and a power supply; we carried out our photocurrent measurements in a probe

#176411 - $15.00 USD Received 18 Sep 2012; revised 15 Nov 2012; accepted 13 Dec 2012; published 10 Jan 2013

station and coupled the incoming monochromatic light through the objective lens of the probe station microscope. The spot size of the light coupled to the devices is about 200 μm, which is smaller than our device mesa.

Here it is worth noting that, considering the geometries used and materials involved in the samples, mask patterns acting as optical scatterers have a very little effect on these EA measurements, because we are looking at the optical signal that is external field dependent. Moreover, since we use single side polished sapphire substrates, any such effect will be minimal due to light diffusion through the unpolished side. Due to the partial compensation of the polarization-induced electrostatic fields inside the well layers by the external electric field, we observed a strong blue shift of the absorption edge and thus, a decrease in the absorption level around the band edge, with increasing external bias. Such an electroabsorption behavior, called reversed quantum-confined Stark effect, has been observed previously [14, 21].

In this study, we consider the photocurrent change at 4 V with respect to 0 V absorption levels, $\Delta i_{ph}(\lambda)$. In the wavelength interval where the blue shift is observed, this gives a figure of merit for comparative electroabsorption performance of these devices. Here, we define the maximum photocurrent change, i.e., $\max[-\Delta i_{ph}(\lambda)]$, over the operating wavelength range, which is related to the electroabsorption performance. Also, the wavelength at which this maximum occurs can be considered as the electroabsorption modulator optimal operating wavelength of the corresponding sample, λ_{EA}. This wavelength where the absorption changes the most via the externally applied electric field is expected to follow the same trend as λ_{PL} for all samples. The related FWHM ($\Delta\lambda_{EA}$) can also be defined as the operation wavelength range, over which the quantum electroabsorption behavior is observed. This quantum effect should correlate correspondingly with the broadening of the PL emission of our quantum structures, since they both are related with the bound states near the bandgap.

In Figs. 5(a) and 5(b), we show the PL peak wavelength (λ_{PL}) and the maximum absorption change wavelength (λ_{EA}) for our epitaxial lateral overgrowth samples, which are consistent with each other. As seen in Fig. 5(c) and 5(d), $\Delta\lambda_{EA}$ also follows the FWHM of PL emission ($\Delta\lambda_{PL}$). Moreover, the level of maximum photocurrent change with the voltage swing from 4 to 0 V, $\max[-\Delta i_{ph}(\lambda)]$, and the PL peak intensity levels, I_{PL}, follow a similar trend, except for a small variation in PL intensities of the samples with 7 and 10 μm stripe width. Also, all these trends correlate well with the carrier lifetimes and the dislocation densities mentioned earlier. Therefore, these analyses show that the EA performance follows similar trends to the essential parameters of the PL spectra (peak position, width and intensity) as well as the photoluminescence lifetimes.

In our experimental measurements, we consistently observe that the lower dislocation density leads to stronger electroabsorption, although this dependence of electroabsorption on dislocation density may not be obvious for those who are more familiar with photoluminescence (e.g., LEDs). As an important remark, our results suggest that the electroabsorption performance of the best performing ELOG structure (4 μm stripe width) is about 3-fold better than its nearest competitor (7 μm stripe width). This performance difference of EA is significantly larger than the ratio of their corresponding PL intensities. Furthermore, this strong electroabsorption is 4.8-fold larger than the Reference sample without ELOG.

Compared to the PL intensity levels, this then suggests that, while keeping the growth window widths constant, EA exhibits larger sensitivity to the decreasing ELOG mask stripe widths, which reduces dislocation density. This observation therefore indicates surprisingly that EA results in the strongest dependence on the mask stripe widths.

#176411 - $15.00 USD Received 18 Sep 2012; revised 15 Nov 2012; accepted 13 Dec 2012; published 10 Jan 2013

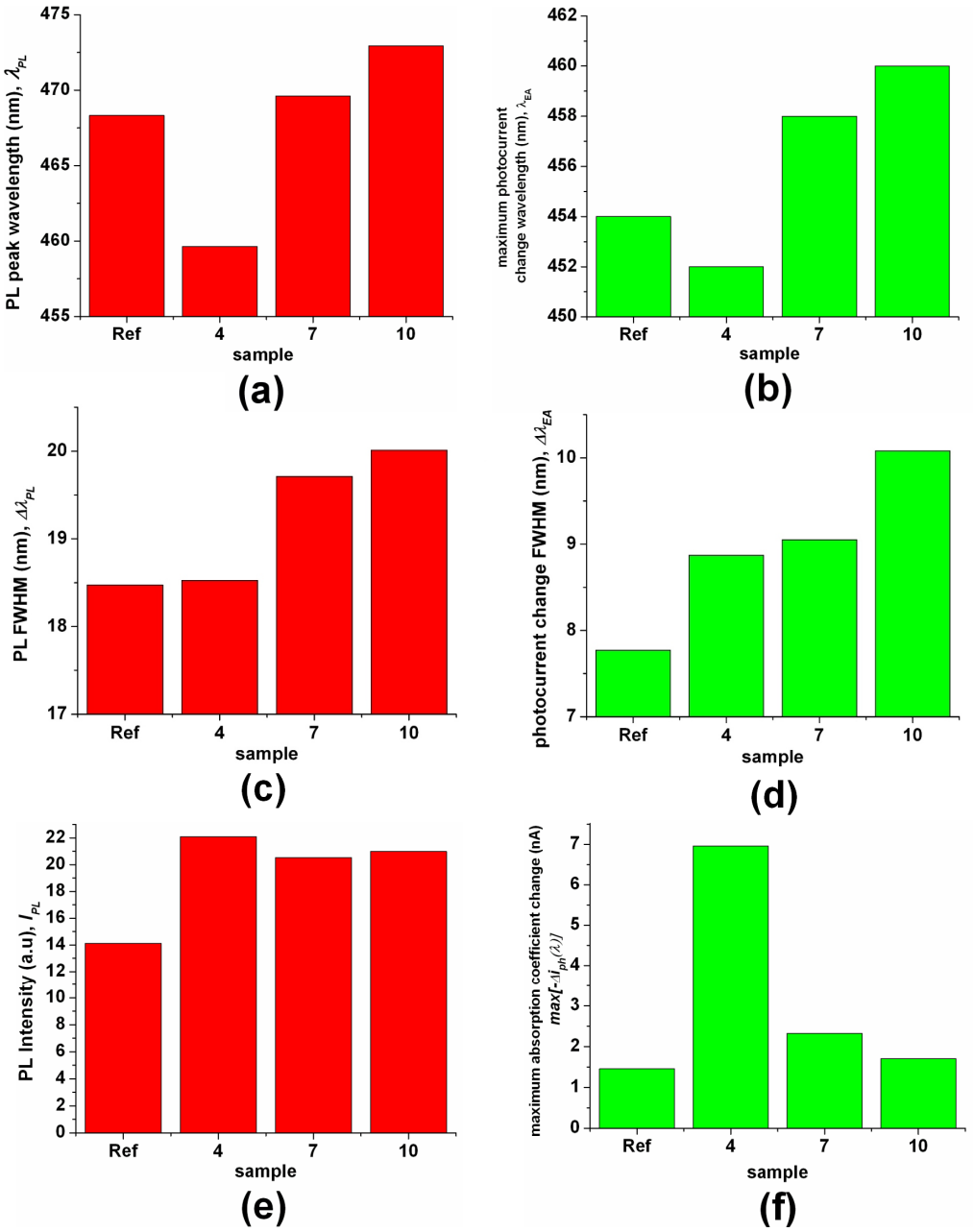

Fig. 5. Comparison of trends in (a) PL peak wavelengths and (b) maximum photocurrent change (electroabsorption) wavelengths; (c) PL peak FWHMs and (d) electroabsorption FWHMs; and (d) PL peak intensities and (e) maximum photocurrent changes among our structures.

We attribute the observed strong dependence of electroabsorption performance on the dislocation density to higher quality quantum well layers with more uniform thickness and more abrupt interfaces in lower dislocation density samples. Also, considering the fact that strain-induced piezoelectric polarization fields (and thus the total polarization-induced electrostatic fields) inside the well layers bend the conduction and valence bands of the low dislocation density samples more compared to others, they yield a narrower effective bandgap, which causes a red shift in the emission and absorption of the *c*-plane grown polar

#176411 - $15.00 USD Received 18 Sep 2012; revised 15 Nov 2012; accepted 13 Dec 2012; published 10 Jan 2013

InGaN/GaN quantum structures. As a result, the 4 μm ELOG sample's shortest emission wavelength can be explained by its lower amount of the residual strain [22,23], which is released at the coalescence sidewalls more compared to other samples [24]. Since this sample has more stripes, there are more coalescence sidewalls available per unit area. Thus, as a result of the increased crystal quality and the reduced residual strain, the electroabsorption performance is the strongest in the 4 μm ELOG sample compared to the reference. With the decreased levels of dislocation density and residual strain, epitaxial lateral overgrowth therefore enables strong electroabsorption in InGaN/GaN multiple quantum wells.

3. Conclusions

In conclusion, the electroabsorption performance is found superior for the ELOG InGaN/GaN quantum structures (with 4 μm ELOG mask stripes) because of its higher crystal quality and a lower level of residual strain compared to the reference without ELOG. Electroabsorption performance of this sample is much significantly stronger than those of the others, as compared to the difference measured in their PL intensities. The electroabsorption operation wavelengths are observed to follow closely their PL peak wavelengths; the same is also true for the case for their spectral widths. Here the results deduced from different and independent experiments are found in good agreement. The experimental results also indicate that the electroabsorption performance and simultaneous emission rates follow similar trends with the crystalline quality and the level of strain released in the coalescence sidewalls. ELOG, with reduced levels of dislocation density, offers an effective approach for achieving strong electroabsorption in InGaN/GaN quantum structures.

Acknowledgments

This work is supported by EC-FP7 N4E NoE and TUBITAK EEEAG 110E010 and 110E217, and in part by NRF-RF-2009-09 and NRF-CRP-6-2010-02. This work is also partially supported by South Korea NRF 2010-616-D00056. H.V.D. acknowledges support from ESF-EURYI and TUBA-GEBIP; and E.S. from TUBITAK BIDEB 2211 and 2214.

#176411 - $15.00 USD Received 18 Sep 2012; revised 15 Nov 2012; accepted 13 Dec 2012; published 10 Jan 2013